

# Quasiparticle Interference of Spin-Triplet Superconductors: Application to UTe<sub>2</sub>

Hans Christiansen<sup>1</sup>, Brian M. Andersen<sup>1</sup>, P. J. Hirschfeld<sup>2</sup>, and Andreas Kreisel<sup>1</sup>

<sup>1</sup>Niels Bohr Institute, University of Copenhagen, DK-2100 Copenhagen, Denmark

<sup>2</sup>Department of Physics, University of Florida, Gainesville, Florida 32611, USA

Quasiparticle interference (QPI) obtained from scanning tunneling microscopy (STM) is a powerful method to help extract the pairing symmetry of unconventional superconductors. We examine the general properties of QPI on surfaces of spin-triplet superconductors, where the properties of the  $\vec{d}$ -vector order parameter and topological surface bound states offer important differences from QPI on spin-singlet superconducting materials. We then apply the theory to a model specific to UTe<sub>2</sub>, and compare the resulting QPI with recent STM measurements. We conclude that the two candidate Cooper pair instabilities  $B_{2u}$  and  $B_{3u}$  exhibit distinct features in the QPI intensity to discriminate these using the experimental data. Characteristic features of the emergent topological surface states protected by mirror symmetries provide further unique signatures to help pinpointing the pairing symmetry channel of UTe<sub>2</sub>.

**Introduction.** Spin-triplet superconductivity (SC) is a fascinating state of matter with long sought-after properties for the development of future possible quantum technologies [1, 2]. SC with spin-triplet Cooper pairs is richer than conventional  $s$ -wave SC in the sense that the condensed order allows for several different flavors, including for example chiral, helical, unitary, and non-unitary order parameters. These phases are symmetry-distinct and identified, for example, by the breaking of mirror or time-reversal symmetries (TRS). An important property of spin-triplet SC is the associated topological surface states (TSS) protected by bulk winding numbers or crystalline symmetries, depending on the flavor of the triplet order, the Fermi surface topology, and the particular surface under consideration [3–6]. Indeed, such TSS and their potential robustness towards perturbations constitute the main desirable property of spin-triplet SC for applications. The existence of these surface states motivates the use of surface-sensitive experimental probes to access and manipulate the electronic surface properties. From a theoretical perspective, this requires the development of realistic surface theories able to capture the emergent TSS from the bulk Hamiltonian.

The heavy-fermion compound UTe<sub>2</sub> is currently under intense investigation due to intrinsic spin-triplet SC phase that may well be realized in its ground state [7–9]. This is deduced from critical magnetic fields larger than the Pauli-limiting field and the absence of a substantial Knight shift upon entering the SC phase [7, 10–12]. At present, the experimental status of the nature of SC in UTe<sub>2</sub> remains controversial, particularly with respect to the position of the point nodes and the possible realization of a chiral (non-unitary) condensate [13–19]. Thus, further experiments and theoretical studies are needed to determine the precise nature of the Cooper pairing in UTe<sub>2</sub>.

Here, we focus on the technique of quasiparticle interference (QPI), an important probe for determining the gap structure of unconventional SC [20–26]. We study the salient properties of QPI for spin-triplet SC in gen-

eral, and UTe<sub>2</sub>, in particular. Generically, QPI in triplet SC feature distinct properties compared to singlet SC, which needs to be taken into account for a proper interpretation of the QPI response. In the spin-singlet case, scattering takes place between states at momenta with the same or opposite signs of the order parameter, giving rise to interference effects that can be used to detect sign-changing singlet SC [27–30]. However, in a triplet SC, the  $\vec{d}$ -vector order parameter plays a crucial role for QPI and yields qualitatively different properties because of the vector nature of the order parameter. In particular, scattering can be suppressed or enhanced due to the direction of the  $\vec{d}$ -vector without direct connection to the magnitude of the  $\vec{d}$ -vector, which determines the energy of the Bogoliubov quasiparticles. Additionally, spin-triplet SC tend to be topological and host unique surface states important for the QPI. We demonstrate these properties of spin-triplet QPI by applying a realistic model of the SC state in UTe<sub>2</sub> [19]. Specifically, we compute both bulk and surface Greens functions in the SC state and obtain the corresponding QPI from impurity scattering. For the particular case of UTe<sub>2</sub>, it is important to address the experimentally relevant (0-11) cleave plane investigated by STM experiments. We find that the TSS offer unique signatures that can help pinpoint the pairing structure. From comparison to available experimental QPI data [26], we conclude that the SC ground state of UTe<sub>2</sub> is likely to reside within the  $B_{3u}$  symmetry channel.

**QPI in spin-triplet superconductors.** Before turning to a specific discussion of QPI in UTe<sub>2</sub>, we provide a general study of the basic properties of QPI in triplet SC, contrasting it to the case of spin-singlet condensates. The starting point is a single-band model with the Bogoliubov-de Gennes (BdG) Hamiltonian

$$\check{H}(\mathbf{k}) = \begin{pmatrix} H_N(\mathbf{k})\sigma_0 & \Delta(\mathbf{k}) \\ \Delta^\dagger(\mathbf{k}) & -H_N^*(-\mathbf{k})\sigma_0 \end{pmatrix}, \quad (1)$$

in the Nambu basis  $\vec{c}_{\mathbf{k}} \equiv (c_{\mathbf{k}\uparrow}, c_{\mathbf{k}\downarrow}, c_{-\mathbf{k}\uparrow}^\dagger, c_{-\mathbf{k}\downarrow}^\dagger)$  with the

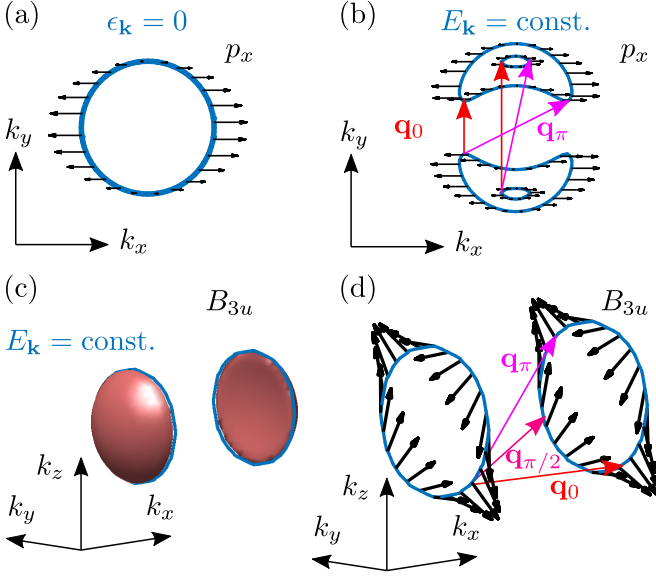


FIG. 1. QPI in triplet superconductors (a) Fermi surface and  $\vec{d}$  vector of a  $p_x$  SC with  $\vec{d} = pk_x \vec{e}_x$  in 2D. (b) Two contours of constant energy of the quasiparticle dispersion  $E_{\mathbf{k}}$ . For small energies, a “banana” close to the nodal point at  $k_x = 0$  occurs such that scattering processes with relative angle 0 between the  $\vec{d}$ -vectors (labeled by  $\mathbf{q}_0$ ) and relative angle  $\pi$  (labeled by  $\mathbf{q}_\pi$ ) are difficult to resolve experimentally. At larger energies  $\mathbf{q}_0$  and  $\mathbf{q}_\pi$  can be more easily resolved and contain information about the relative direction of the  $\vec{d}$ -vector. (c) 3D analogon for a  $B_{3u}$  state on a spherical Fermi surface, compare Fig. S3 in the SM. With the vector  $\vec{d}_{B_{3u}} = (p_1 k_x k_y k_z, p_2 k_z, p_3 k_y)$ , there are point nodes at the  $k_x$  axis such that at small energy the contours of constant energy form small “lenticles” centered around the  $k_x$  axis (red surface). Scattering at this energy is dominated by processes from the edges (blue lines) similar to the scattering processes of the tips of the “bananas” in two dimensions. (d) The  $\vec{d}$ -vector along these lines winds around such that there are scattering processes with all relative angles between the  $\vec{d}$ -vectors. Three example vectors with relative angle of the  $\vec{d}$ -vectors of 0,  $\pi/2$  and  $\pi$  are shown. At low energies, the “lenticles” (and therefore the blue circles of large DOS) are small and  $\mathbf{q}_0$  and  $\mathbf{q}_\pi$  may not be resolvable experimentally, similar to the 2D case.

normal state Hamiltonian  $H_N(\mathbf{k}) = \xi_{\mathbf{k}} = \epsilon_{\mathbf{k}} - \mu$ , where  $\epsilon_{\mathbf{k}}$  is a dispersion and  $\mu$  the chemical potential. In terms of a  $\vec{d}$ -vector, the triplet order parameter is given by

$$\Delta(\mathbf{k}) = (\vec{d}_{\mathbf{k}} \cdot \vec{\sigma}) i \sigma_y, \quad (2)$$

with quasiparticle energies  $E_{\mathbf{k}} = \pm \sqrt{\xi_{\mathbf{k}}^2 + |\vec{d}_{\mathbf{k}}|^2}$ . The momentum- and energy-resolved density modulations for scattering from  $\mathbf{k}_F$  to  $\mathbf{k}_F + \mathbf{q}_i$  from a non-magnetic impurity of strength  $V_0$  are given by

$$\delta\rho(\mathbf{k}_F, \mathbf{q}_i, \omega) = -2 \frac{V_0}{\pi} \text{Im} \left( \frac{(\omega + i\delta)^2 - \vec{d}_{\mathbf{k}_F} \cdot \vec{d}_{\mathbf{k}_F + \mathbf{q}_i}^*}{[(\omega + i\delta)^2 - |\vec{d}_{\mathbf{k}_F}|^2]^2} \right), \quad (3)$$

as derived in the supplementary information (SM). Here, we have used the fact that dominant contributions occur from elastic scattering between two saddle points in the quasiparticle dispersion with  $E_{\mathbf{k}} = E_{\mathbf{k}+\mathbf{q}_i}$ . In addition, we have summed over spin, since we restrict our discussion to non-spin-polarized tunneling here. The contribution from a cross product term,  $\vec{d}_{\mathbf{k}_F} \times \vec{d}_{\mathbf{k}_F + \mathbf{q}_i}^*$ , which can be nonzero even in the non-unitary case, drops out, see SM. The density modulations  $\delta\rho$  in a singlet superconductor[31] contain a term  $\Delta_{\mathbf{k}} \Delta_{\mathbf{k}+\mathbf{q}}$ , making the relative sign of the order parameter accessible in QPI. For the triplet superconductor, the corresponding expression, Eq. (3), exhibits the term  $\vec{d}_{\mathbf{k}_F} \cdot \vec{d}_{\mathbf{k}_F + \mathbf{q}_i}^*$  which can take all values from  $-|\vec{d}_{\mathbf{k}_F}|^2$  to  $|\vec{d}_{\mathbf{k}_F}|^2$ .

For the simple  $p_x$  superconductor, we have scattering processes labelled by  $\mathbf{q}_\pi$  ( $\mathbf{q}_0$ ) where this scalar product is negative (positive), see Fig. 1 (b). The antisymmetric density modulations  $\rho^-(\omega) = \rho(\omega) - \rho(-\omega)$  as introduced in Ref.[31], exhibit no sign change (a sign change) from zero energy to the magnitude  $|\vec{d}_{\mathbf{k}_F}|$  for  $\mathbf{q}_\pi$  ( $\mathbf{q}_0$ ) similar to the singlet case with (without) sign change in the singlet order parameter  $\Delta_{\mathbf{k}}$ .

This argument remains valid in three dimensions (3D) where for the  $B_{3u}$  order parameter, the nodal points at zero energy evolve to contours of constant energy with  $E_{\mathbf{k}} = \omega$  of “lenticle” shape (Fig. 1 (c)). Dominant scattering comes from the edges of the lenticles (blue line) where the  $\vec{d}$ -vector winds as shown in Fig. 1 (d). Thus, we have three qualitative different behaviors of antisymmetric density modulations,  $\rho^-(\omega)$ : If the  $\vec{d}$ -vectors are perpendicular, as for example for  $\mathbf{q}_{\pi/2}$ , there is no signal. If the relative direction of  $\vec{d}_{\mathbf{k}_F}$  and  $\vec{d}_{\mathbf{k}_F + \mathbf{q}_i}^*$  is parallel (antiparallel), the corresponding antisymmetric density modulations,  $\rho^-(\omega)$ , exhibit a sign change (no sign change) from zero energy to the magnitude  $|\vec{d}_{\mathbf{k}_F}|$  similar to the singlet case [31]. However, when considering scattering at low energies, i.e. for investigating the location of possible nodes, one integrates over momenta that connect  $\mathbf{k}$ -points with opposite directions of the  $\vec{d}$ -vector such that one averages over this quantity. Consequently, it is not possible to deduce the relative direction of the  $\vec{d}$ -vector close to nodal points. We note that the change of the direction of the  $\vec{d}$ -vector is imposed by symmetry, since the  $\vec{d}$ -vector changes sign across the nodal position, as shown in Fig. 1. In the SM, we discuss the  $\vec{d}$ -vector structure of other example order parameters and scattering vectors  $\mathbf{q}_0$  and  $\mathbf{q}_\pi$ .

**QPI in  $\text{UTe}_2$ .**— As a concrete timely example of QPI in a spin-triplet SC, we turn to the SC ground state of  $\text{UTe}_2$ .  $\text{UTe}_2$  is a body-centered orthorhombic material with  $D_{2h}$  point group symmetry, allowing four symmetry-distinct odd-parity spin-triplet order parameters in the case of strong spin-orbit coupling (SOC):  $A_u$ ,  $B_{1u}$ ,  $B_{2u}$ , and  $B_{3u}$ . The BdG Hamiltonian and the order parameter are still given by Eq. (1) and (2), but  $H_N(\mathbf{k})$  is

now a  $4 \times 4$  matrix due to U or Te sublattices, similar to the formulation of the model found in Ref. [19]. The normal-state Hamiltonian  $H_N(\mathbf{k})$  is based on density functional theory (DFT) calculations and a four-band tight-binding fit matching recent quantum oscillation measurements [17, 32, 33]. The four allowed SC odd-parity irreps restrict the possible pairing structures in sublattice and U/Te space and specify the final applied microscopic model for the SC phases of  $\text{UTe}_2$ . For all the details of model parameters and basis functions, we refer to Ref. [19] and the SM. STM on  $\text{UTe}_2$  tunnels into the (0-11) cleave plane [18, 26, 34]. Thus, for comparison to experiments, theory necessarily needs to obtain the electronic states present at that particular surface. This is especially important for spin-triplet SC, where the odd-parity of the pair wavefunction  $\Delta(-\mathbf{k}) = -\Delta(\mathbf{k})$  tends to generate new low-energy Andreev states bound to the surfaces [2, 4–6, 19, 35–37]. The topological nature of these surface states depends on the topology of the Fermi surface. For the case of  $\text{UTe}_2$  with open cylindrical Fermi sheets, they are weak and only protected by time-reversal and mirror symmetry along one direction of the (0-11) plane [19]. Nevertheless, *bona fide* massless Majorana surface modes emanating from time-reversal invariant momenta (TRIM) are generated in the present case, and hence relevant for the discussion of STM tunneling spectroscopy. Therefore, we compute both the bulk  $G_b(\mathbf{k}^\parallel, \omega)$  and surface  $G_s(\mathbf{k}^\parallel, \omega)$  Green's functions. Here,  $\mathbf{k}^\parallel$  refers to the momentum parallel to the surface i.e.  $\mathbf{k}^\parallel = k_x \vec{m}_x + k_{c^*} \vec{m}_{c^*}$ , with  $\vec{m}_x = (1/a, 0, 0)$  and  $\vec{m}_{c^*} = (0, 1/b, 1/c)$ . For a detailed discussion of  $G_s(\mathbf{k}^\parallel, \omega)$  and the topological aspects of the surface states, we refer to the SM and Refs. [6, 19, 37, 38].

Having obtained the homogeneous Green's functions, we turn to QPI signals induced by impurities on the (0-11) surface. As shown in the SM, the generalization of the density modulation from an impurity with strength  $V_0$  in Eq. (3) for the multi-band case is

$$\delta\rho_\beta(\mathbf{q}^\parallel, \omega) = -\frac{V_0}{2\pi i} (f_\beta(\mathbf{q}^\parallel, \omega) - f_\beta^*(-\mathbf{q}^\parallel, \omega)), \quad (4)$$

with

$$f_\beta(\mathbf{q}^\parallel, \omega) = \sum_{\mathbf{k}^\parallel} \text{Tr} \left( \tau_e G_s(\mathbf{k}^\parallel + \mathbf{q}^\parallel, \omega) \tau_3 P_\beta G_s(\mathbf{k}^\parallel, \omega) \right), \quad (5)$$

where  $\tau_3$  is the third Pauli matrix in Nambu space,  $\tau_e = (\tau_0 + \tau_3)/2$  projects onto the electronic sector, and  $P_\beta$  is a projector onto U/Te and one of the sublattice degrees of freedom. The total density modulation is computed as  $\delta\rho(\mathbf{q}^\parallel, \omega) = \sum_\beta |\rho_\beta(\mathbf{q}^\parallel, \omega)|$  where the absolute value arises from the assumption of homogeneously distributed impurities.

To set the stage for the following discussion on QPI in  $\text{UTe}_2$ , we show in Fig. 2(a) the bulk bands at  $k_z = 0$  with nodes highlighted for  $B_{2u}$  ( $B_{3u}$ ). The symmetry-imposed

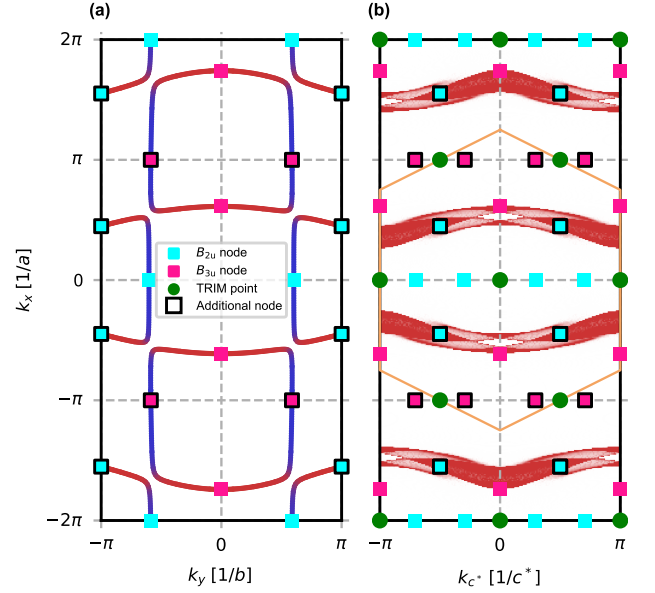


FIG. 2. (a) Fermi surface at  $k_z = 0$  with red (blue) bulk bands dominated by U (Te) orbital content. (b) The red U bands dominate the band structure at the (0-11) surface. The locations of symmetry-imposed and additional nodes for both  $B_{2u}$  and  $B_{3u}$  have been indicated in both panels, along with the TRIM points relevant for the TSS. The orange lines in (b) indicate the surface BZ.

nodes are located along the  $k_x$  ( $k_y$ ) axis, whereas additional nodes are present at other locations of the Fermi surface, as shown in Fig. 2 and elaborated in the SM. Figure 2(b) displays the bands projected to the experimentally relevant (0-11) cleave plane, and the positions of the nodes and the TRIM points on that surface. As seen, only the U-dominated states lead to distinct bands on the surface. By contrast, the Te bands produce an almost constant background weight due to the angle of the cleave plane and the flat dispersion of those bands, see SM for further details of the (0-11) coordinates and surface BZ. In the presence of impurities, a characteristic normal state QPI pattern emerges from scattering between the bands shown in Fig. 2(b). We provide a discussion of the normal-state QPI in the SM, and focus here on the salient QPI signatures arising from entering the SC state. In the SC phase, low-energy QPI is strongly restricted due to the gap, but additional complexity arises for triplet SC due to the structure of the  $\vec{d}$ -vector (see above) and the emergence of TSS.

Figure 3(a,b) display the spectral functions of both the bulk and surface for the case of  $B_{2u}$  and  $B_{3u}$  SC, respectively. As seen from comparison to Fig. 2(b), spectral intensity exists both near the surface-projected nodes from the bulk bands and at the TRIM points due to the emergent TSS. Disorder generates scattering between these quasiparticle states, producing a spectacle of interference

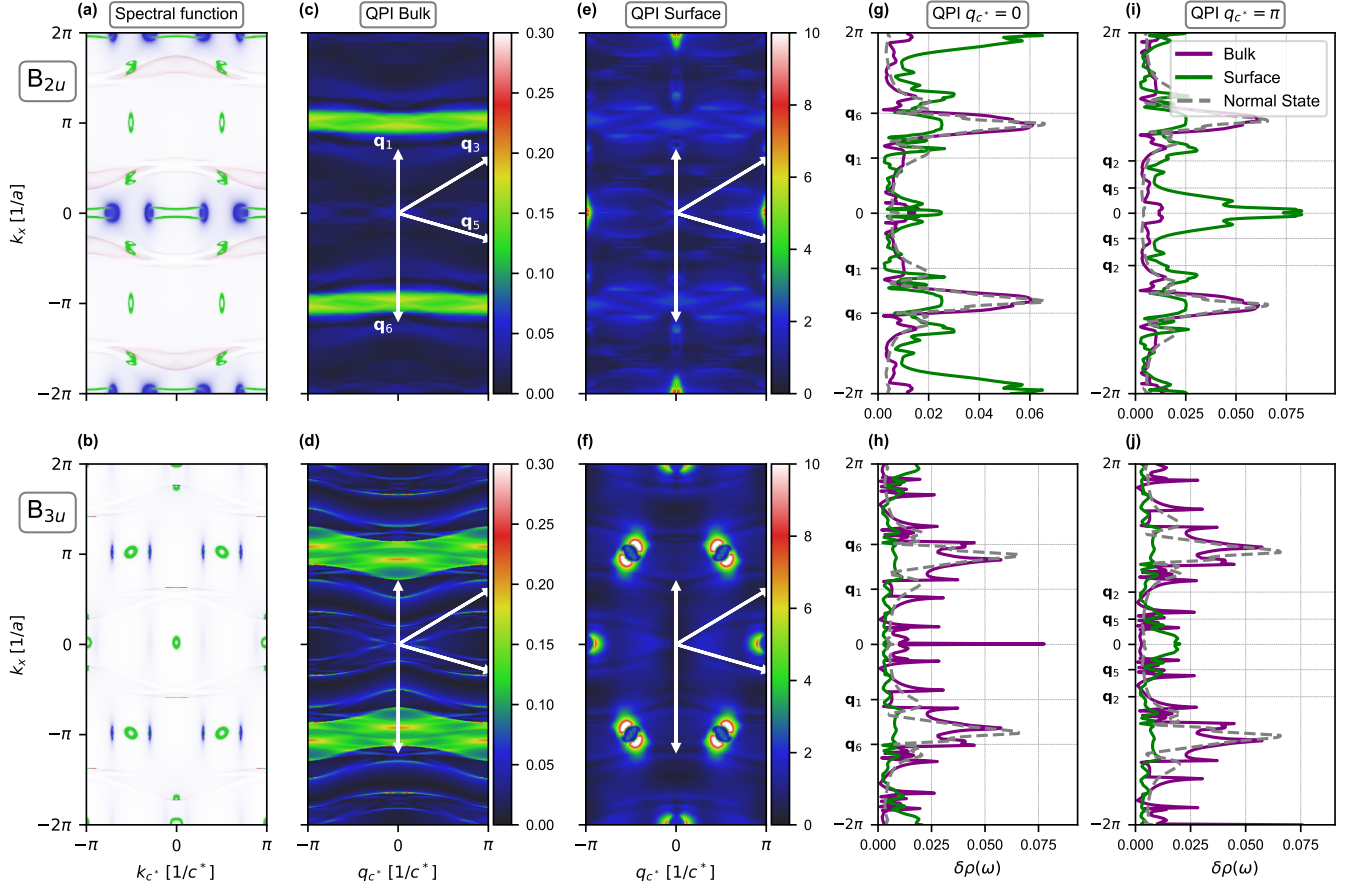


FIG. 3. QPI signal  $\delta\rho(\mathbf{q}^{\parallel}, \omega)$  and spectral functions  $A_{s/b}(\mathbf{q}^{\parallel}, \omega) = -\frac{1}{\pi}\text{Im}G_{s/b}(\mathbf{q}^{\parallel}, \omega)$  on the (0-11) surface of  $\text{UTe}_2$  in the  $B_{2u}$  and  $B_{3u}$  phases. (a-b) The bulk U (red) and Te (blue) spectral functions along with the surface states (green). (c,d) [e,f] QPI versus surface momentum at  $\omega = 0.05\Delta_0$  including the surface-projected bulk [surface] states. Characteristic scattering vectors  $\mathbf{q}_i$  are indicated by arrows. (g,h) [(i,j)] Momentum cuts of the respective panels (c,d) [e,f] at  $q_{c^*} = 0, \pi$ . In panels (g-j) we have also indicated the locations of  $\mathbf{q}_i$ . As seen, only the  $B_{3u}$  pairing symmetry features significant enhancements at  $\mathbf{q}_1$  and  $\mathbf{q}_5$  compared to the normal state QPI response. In panels (c-f) the plots are in units of  $V_0/\text{eV}^2$  while in panels (g-j) the density modulations have been normalized such that  $\sum_{\mathbf{q}^{\parallel}} \delta\rho(\mathbf{q}^{\parallel}, \omega) = 1$ .

patterns shown in Fig. 3(c-f). To clearly decipher the resulting QPI results, we show the QPI patterns arising from bulk and surface states separately in Figs. 3(c,d) and 3(e,f), respectively. QPI linecuts at  $k_{c^*} = 0, \pi$  are shown for both the normal state and the  $B_{2u}$  and  $B_{3u}$  SC cases in Figs. 3(g-j). From the QPI data shown in Fig. 3, we draw two main conclusions: 1)  $B_{3u}$  is the most likely pairing channel realized in  $\text{UTe}_2$ , and 2) distinctive QPI patterns from TSS offer additional means to distinguish between  $B_{2u}$  and  $B_{3u}$  SC.

Conclusion 1) results from the fact that the enhanced scattering channels dubbed  $\mathbf{q}_1$  and  $\mathbf{q}_5$  in Ref. [26], as shown explicitly in Fig. 3, are generically only significantly enhanced compared to the normal state in the  $B_{3u}$  phase, see also Ref. [39]. This is because only for  $B_{3u}$ , these scattering vectors arise from Bogoliubov quasiparticle scattering between symmetry-imposed nodes. In the SM section, we discuss a special (fine-tuned) case where

$B_{2u}$  exhibits scattering at  $\mathbf{q}_1$  and  $\mathbf{q}_5$  from the additional nodes. Even in that case, however, the conclusion remains that only  $B_{3u}$  features enhanced QPI response at  $\mathbf{q}_1$  and  $\mathbf{q}_5$  compared to the normal state. Conclusion 2) arises from the fact that only the  $B_{2u}$  state features Majorana flatband TSS whereas  $B_{3u}$  supports Majorana-Dirac TSS dispersions, see Fig. 3(e,f) and Fig. 3(g-j). The origin of this qualitative difference can be traced to the different properties of  $B_{2u}$  and  $B_{3u}$  under mirror along  $k_x$  [19]. For the resulting QPI patterns, this leads to distinct flat bands (cones) of scattering intensity for  $B_{2u}$  and  $B_{3u}$ , respectively, as seen from Fig. 3(e,f). The low-energy quasiparticles close to the TRIM point  $i$  can be described by an effective Hamiltonian  $H_{i,\text{eff}}(\mathbf{k}^{\parallel}) = \tilde{d}_i(\mathbf{k}^{\parallel}) \cdot \vec{\sigma}$  using the two zero-energy states at the TRIM point as basis states. The spin polarization of the TSS determines their effective  $\tilde{d}_i$ -vector which, in turn, strongly affects the surface QPI. The difference to the simple  $\vec{d}$ -vectors



discussed in Fig. 1 lies in the possibility to have different winding directions on distinct Dirac cones. This averages out the QPI intensity for a  $\mathbf{q}$ -vector connecting the centers of the Dirac dispersions. The texture of this  $\vec{d}$ -vector near the TRIM points allows to understand the main features of the QPI intensity in Fig. 3(e,f) with the following observation: The relative direction of  $\vec{d}_i(\mathbf{k}^\parallel)$  and  $\vec{d}_j(\mathbf{k}^\parallel + \mathbf{q}^\parallel)$  for a given scattering vector  $\mathbf{q}^\parallel$  deduces the magnitude of the expected scattering amplitude in QPI, see SM.

In comparison with the experimental QPI data available on  $\text{UTe}_2$  [26], no distinctive TSS features stand out near the TRIM points. This may be due to the fact that the crystalline TSS in the present case are only protected by TRS and one mirror, making their distinctive features fragile to actual concentrations of disorder on the surface. A large resulting featureless spectral weight from these surface states may be related to the large background conductance seen experimentally [18, 26, 40–42]. Additionally,  $\text{UTe}_2$  is known to host a weak surface charge density wave (CDW) which is manifested by the nondispersive QPI peaks  $\mathbf{q}_2$ ,  $\mathbf{q}_6$ , and possibly  $\mathbf{q}_1$  [43–46]. Since the model applied in this work already contains enhanced scattering at those wave vectors in the normal state, the surface CDW may arise from favorable nesting properties at those momenta transfer. It constitutes an interesting future study to include the weak surface CDW explicitly in the calculations of the QPI. We do not, however, anticipate this to qualitatively alter our conclusions of the QPI response in the superconducting state.

**Conclusions.**— We have provided a general study of QPI in spin-triplet superconductors and discussed the differences from the spin-singlet case arising from the vectorial nature of the triplet order parameter. We focused on the timely example of  $\text{UTe}_2$ , and computed the QPI response of this material on the experimentally relevant (0-11) cleave plane. From comparison to currently available experimental SC QPI data [26], we conclude that  $B_{3u}$  pairing appears most likely as the ground state symmetry of SC in  $\text{UTe}_2$ . Distinct topological surface states in the cases of  $B_{2u}$  and  $B_{3u}$  pairing offer an additional possibility for distinguishing these phases in future STM experiments on pristine surfaces.

**Acknowledgements.**— We acknowledge discussions with J. C. Séamus Davis and Max Geier. H. C. acknowledges support from the Novo Nordisk Foundation grant NNF20OC0060019. A. K. acknowledges support by the Danish National Committee for Research Infrastructure (NUFI) through the ESS-Lighthouse Q-MAT.

---

[1] Sankar Das Sarma, Michael Freedman, and Chetan Nayak, “Majorana zero modes and topological quantum computation,” *npj Quantum Information* **1**, 15001

(2015).

[2] Masatoshi Sato and Satoshi Fujimoto, “Majorana Fermions and topology in superconductors,” *Journal of the Physical Society of Japan* **85**, 072001 (2016).

[3] Masatoshi Sato, “Topological odd-parity superconductors,” *Phys. Rev. B* **81**, 220504 (2010).

[4] Timothy H. Hsieh and Liang Fu, “Majorana Fermions and Exotic Surface Andreev Bound States in Topological Superconductors: Application to  $\text{Cu}_x\text{Bi}_2\text{Se}_3$ ,” *Phys. Rev. Lett.* **108**, 107005 (2012).

[5] Jun Ishizuka, Shuntaro Sumita, Akito Daido, and Youichi Yanase, “Insulator-Metal Transition and Topological Superconductivity in  $\text{UTe}_2$  from a First-Principles Calculation,” *Phys. Rev. Lett.* **123**, 217001 (2019).

[6] Henrik S. Røising, Max Geier, Andreas Kreisel, and Brian M. Andersen, “Thermodynamic transitions and topology of spin-triplet superconductivity: Application to  $\text{UTe}_2$ ,” *Phys. Rev. B* **109**, 054521 (2024).

[7] Sheng Ran, Chris Eckberg, Qing-Ping Ding, Yuji Furukawa, Tristin Metz, Shanta R. Saha, I-Lin Liu, Mark Zic, Hyunsoo Kim, Johnpierre Paglione, and Nicholas P. Butch, “Nearly ferromagnetic spin-triplet superconductivity,” *Science* **365**, 684–687 (2019).

[8] D. Aoki, J.-P. Brison, J. Flouquet, K. Ishida, G. Knebel, Y. Tokunaga, and Y. Yanase, “Unconventional superconductivity in  $\text{UTe}_2$ ,” *Journal of Physics: Condensed Matter* **34**, 243002 (2022).

[9] Sylvia K Lewin, Corey E Frank, Sheng Ran, Johnpierre Paglione, and Nicholas P Butch, “A review of  $\text{UTe}_2$  at high magnetic fields,” *Reports on Progress in Physics* **86**, 114501 (2023).

[10] Dai Aoki, Ai Nakamura, Fuminori Honda, DeXin Li, Yoshiya Homma, Yusei Shimizu, Yoshiki J. Sato, Georg Knebel, Jean-Pascal Brison, Alexandre Pourret, Daniel Braithwaite, Gerard Lapertot, Qun Niu, Michal Vališka, Hisatomo Harima, and Jacques Flouquet, “Unconventional superconductivity in heavy Fermion  $\text{UTe}_2$ ,” *Journal of the Physical Society of Japan* **88**, 043702 (2019).

[11] Genki Nakamine, Shunsaku Kitagawa, Kenji Ishida, Yo Tokunaga, Hironori Sakai, Shinsaku Kambe, Ai Nakamura, Yusei Shimizu, Yoshiya Homma, Dexin Li, Fuminori Honda, and Dai Aoki, “Superconducting properties of heavy Fermion  $\text{UTe}_2$  revealed by  $^{125}\text{Te}$ -nuclear magnetic resonance,” *Journal of the Physical Society of Japan* **88**, 113703 (2019).

[12] Hiroki Matsumura, Hiroki Fujibayashi, Katsuki Kinjo, Shunsaku Kitagawa, Kenji Ishida, Yo Tokunaga, Hironori Sakai, Shinsaku Kambe, Ai Nakamura, Yusei Shimizu, Yoshiya Homma, Dexin Li, Fuminori Honda, and Dai Aoki, “Large Reduction in the a-axis Knight Shift on  $\text{UTe}_2$  with  $T_c = 2.1$  K,” *Journal of the Physical Society of Japan* **92**, 063701 (2023).

[13] Kota Ishihara, Masaki Roppongi, Masayuki Kobayashi, Kumpei Imamura, Yuta Mizukami, Hironori Sakai, Petr Opletal, Yoshifumi Tokiwa, Yoshinori Haga, Kenichiro Hashimoto, and Takasada Shibauchi, “Chiral superconductivity in  $\text{UTe}_2$  probed by anisotropic low-energy excitations,” *Nature Communications* **14**, 2966 (2023).

[14] M. O. Ajeesh, M. Bordelon, C. Girod, S. Mishra, F. Ronning, E. D. Bauer, B. Maierov, J. D. Thompson, P. F. S. Rosa, and S. M. Thomas, “Fate of Time-Reversal Symmetry Breaking in  $\text{UTe}_2$ ,” *Phys. Rev. X* **13**, 041019 (2023).

[15] Shota Suetsugu, Masaki Shimomura, Masashi

- Kamimura, Tomoya Asaba, Hiroto Asaeda, Yuki Kosuge, Yuki Sekino, Shun Ikemori, Yuichi Kasahara, Yuhki Kohsaka, Minhyea Lee, Youichi Yanase, Hironori Sakai, Petr Opletal, Yoshifumi Tokiwa, Yoshinori Haga, and Yuji Matsuda, “Fully gapped pairing state in spin-triplet superconductor  $\text{UTe}_2$ ,” *Science Advances* **10**, eadk3772 (2024).
- [16] Ian M. Hayes, Tristin E. Metz, Corey E. Frank, Shanta R. Saha, Nicholas P. Butch, Vivek Mishra, Peter J. Hirschfeld, and Johnpierre Paglione, “Robust nodal behavior in the thermal conductivity of superconducting  $\text{UTe}_2$ ,” *arXiv e-prints*, arXiv:2402.19353 (2024), arXiv:2402.19353 [cond-mat.supr-con].
- [17] Florian Theuss, Avi Shragai, Gaël Grissonnanche, Ian M. Hayes, Shanta R. Saha, Yun Suk Eo, Alonso Suarez, Tatsuya Shishidou, Nicholas P. Butch, Johnpierre Paglione, and B. J. Ramshaw, “Single-component superconductivity in  $\text{UTe}_2$  at ambient pressure,” *Nature Physics* **20**, 1124–1130 (2024).
- [18] Qiangqiang Gu, Shuqiu Wang, Joseph P. Carroll, Kuanysh Zhussupbekov, Christopher Broyles, Sheng Ran, Nicholas P. Butch, Shanta Saha, Johnpierre Paglione, Xiaolong Liu, J. C. Séamus Davis, and Dung-Hai Lee, “Pair Wavefunction Symmetry in  $\text{UTe}_2$  from Zero-Energy Surface State Visualization,” *arXiv e-prints*, arXiv:2501.16636 (2025), arXiv:2501.16636 [cond-mat.supr-con].
- [19] Hans Christiansen, Max Geier, Brian M. Andersen, and Andreas Kreisel, “Nodal superconducting gap structure and topological surface states of  $\text{UTe}_2$ ,” *arXiv e-prints*, arXiv:2503.11603 (2025), arXiv:2503.11603 [cond-mat.supr-con].
- [20] J. E. Hoffman, K. McElroy, D.-H. Lee, K. M. Lang, H. Eisaki, S. Uchida, and J. C. Davis, “Imaging Quasiparticle Interference in  $\text{Bi}_2\text{Sr}_2\text{CaCu}_2\text{O}_{8+x}$ ,” *Science* **297**, 1148–1151 (2002).
- [21] Pegor Aynajian, Eduardo H. da Silva Neto, András Gyenis, Ryan E. Baumbach, J. D. Thompson, Zachary Fisk, Eric D. Bauer, and Ali Yazdani, “Visualizing heavy fermions emerging in a quantum critical Kondo lattice,” *Nature* **486**, 201–206 (2012).
- [22] M. P. Allan, A. W. Rost, A. P. Mackenzie, Yang Xie, J. C. Davis, K. Kihou, C. H. Lee, A. Iyo, H. Eisaki, and T.-M. Chuang, “Anisotropic Energy Gaps of Iron-Based Superconductivity from Intraband Quasiparticle Interference in  $\text{LiFeAs}$ ,” *Science* **336**, 563–567 (2012).
- [23] P. O. Sprau, A. Kostin, A. Kreisel, A. E. Böhmer, V. Taufour, P. C. Canfield, S. Mukherjee, P. J. Hirschfeld, B. M. Andersen, and J. C. Séamus Davis, “Discovery of orbital-selective Cooper pairing in  $\text{FeSe}$ ,” *Science* **357**, 75–80 (2017).
- [24] Zengyi Du, Xiong Yang, Dustin Altenfeld, Qiangqiang Gu, Huan Yang, Ilya Eremin, Peter J. Hirschfeld, Igor I. Mazin, Hai Lin, Xiyu Zhu, and Hai-Hu Wen, “Sign reversal of the order parameter in  $(\text{Li}_{1-x}\text{Fe}_x)\text{OHFe}_{1-y}\text{Zn}_y\text{Se}$ ,” *Nature Physics* **14**, 134–139 (2018).
- [25] A. Kostin, P. O. Sprau, A. Kreisel, Yi Xue Chong, A. E. Böhmer, P. C. Canfield, P. J. Hirschfeld, B. M. Andersen, and J. C. Séamus Davis, “Imaging orbital-selective quasiparticles in the Hund’s metal state of  $\text{FeSe}$ ,” *Nature Materials* **17**, 869–874 (2018).
- [26] Shuqiu Wang, Kuanysh Zhussupbekov, Joseph P. Carroll, Bin Hu, Xiaolong Liu, Emile Pangburn, Adeline Crépieux, Catherine Pepin, Christopher Broyles, Sheng Ran, Nicholas P. Butch, Shanta Saha, Johnpierre Paglione, Cristina Bena, J. C. Séamus Davis, and Qiangqiang Gu, “Imaging Odd-Parity Quasiparticle Interference in the Superconductive Surface State of  $\text{UTe}_2$ ,” *arXiv e-prints*, arXiv:2503.17761 (2025), arXiv:2503.17761 [cond-mat.supr-con].
- [27] Qiang-Hua Wang and Dung-Hai Lee, “Quasiparticle scattering interference in high-temperature superconductors,” *Phys. Rev. B* **67**, 020511 (2003).
- [28] L. Capriotti, D. J. Scalapino, and R. D. Sedgewick, “Wave-vector power spectrum of the local tunneling density of states: Ripples in a d-wave sea,” *Phys. Rev. B* **68**, 014508 (2003).
- [29] Tamara S. Nunner, Wei Chen, Brian M. Andersen, Ashot Melikyan, and P. J. Hirschfeld, “Fourier transform spectroscopy of  $d$ -wave quasiparticles in the presence of atomic scale pairing disorder,” *Phys. Rev. B* **73**, 104511 (2006).
- [30] A. Kreisel, Peayush Choubey, T. Berlijn, W. Ku, B. M. Andersen, and P. J. Hirschfeld, “Interpretation of Scanning Tunneling Quasiparticle Interference and Impurity States in Cuprates,” *Phys. Rev. Lett.* **114**, 217002 (2015).
- [31] P. J. Hirschfeld, D. Altenfeld, I. Eremin, and I. I. Mazin, “Robust determination of the superconducting gap sign structure via quasiparticle interference,” *Phys. Rev. B* **92**, 184513 (2015).
- [32] A. G. Eaton, T. I. Weinberger, N. J. M. Popiel, Z. Wu, A. J. Hickey, A. Cabala, J. Pospíšil, J. Prokleška, T. Haidamak, G. Bastien, P. Opletal, H. Sakai, Y. Haga, R. Nowell, S. M. Benjamin, V. Sechovský, G. G. Lonzarich, F. M. Grosche, and M. Vališka, “Quasi-2D Fermi surface in the anomalous superconductor  $\text{UTe}_2$ ,” *Nature Communications* **15**, 223 (2024).
- [33] T. I. Weinberger, Z. Wu, D. E. Graf, Y. Skourski, A. Cabala, J. Pospíšil, J. Prokleška, T. Haidamak, G. Bastien, V. Sechovský, G. G. Lonzarich, M. Vališka, F. M. Grosche, and A. G. Eaton, “Quantum Interference between Quasi-2D Fermi Surface Sheets in  $\text{UTe}_2$ ,” *Phys. Rev. Lett.* **132**, 266503 (2024).
- [34] Lin Jiao, Sean Howard, Sheng Ran, Zhenyu Wang, Jorge Olivares Rodriguez, Manfred Sigrist, Ziqiang Wang, Nicholas P. Butch, and Vidya Madhavan, “Chiral superconductivity in heavy-fermion metal  $\text{UTe}_2$ ,” *Nature* **579**, 523–527 (2020).
- [35] L. J. Buchholtz and G. Zwirgagl, “Identification of  $p$ -wave superconductors,” *Phys. Rev. B* **23**, 5788–5796 (1981).
- [36] Max Geier, Piet W. Brouwer, and Luka Trifunovic, “Symmetry-based indicators for topological Bogoliubov-de Gennes Hamiltonians,” *Phys. Rev. B* **101**, 245128 (2020).
- [37] Jushin Tei, Takeshi Mizushima, and Satoshi Fujimoto, “Possible realization of topological crystalline superconductivity with time-reversal symmetry in  $\text{UTe}_2$ ,” *Phys. Rev. B* **107**, 144517 (2023).
- [38] M P Lopez Sancho, J M Lopez Sancho, J M L Sancho, and J Rubio, “Highly convergent schemes for the calculation of bulk and surface Green functions,” *Journal of Physics F: Metal Physics* **15**, 851 (1985).
- [39] Adeline Crépieux, Emile Pangburn, Shuqiu Wang, Kuanysh Zhussupbekov, Joseph P. Carroll, Bin Hu, Qiangqiang Gu, J. C. Séamus Davis, Catherine P’épin, and Cristina Bena, “Quasiparticle interference and spectral function of the  $\text{UTe}_2$  superconductive sur-

- face band,” *arXiv e-prints*, [arXiv:2503.17762](#) (2025), [arXiv:2503.17762 \[cond-mat.supr-con\]](#).
- [40] Zhongzheng Yang, Fanbang Zheng, Dingsong Wu, Bin-Bin Zhang, Ning Li, Wenhui Li, Chaofan Zhang, Guang-Ming Zhang, Xi Chen, Yulin Chen, and Shichao Yan, “Magnetization-induced symmetry breaking in the superconducting vortices of  $\text{UTe}_2$ ,” *arXiv e-prints*, [arXiv:2503.13143](#) (2025), [arXiv:2503.13143 \[cond-mat.supr-con\]](#).
- [41] Ruotong Yin, Yuanji Li, Zengyi Du, Dengpeng Yuan, Shiyuan Wang, Jiashuo Gong, Mingzhe Li, Ziyuan Chen, Jiakang Zhang, Yuguang Wang, Ziwei Xue, Xinchun Lai, Shiyong Tan, Da Wang, Qiang-Hua Wang, Dong-Lai Feng, and Ya-Jun Yan, “Yin-Yang vortex on  $\text{UTe}_2$  (011) surface,” *arXiv e-prints*, [arXiv:2503.21506](#) (2025), [arXiv:2503.21506 \[cond-mat.supr-con\]](#).
- [42] Nileema Sharma, Matthew Toole, James McKenzie, Fangjun Cheng, Sean Michael Thomas, Priscila F. S. Rosa, Yi-Ting Hsu, and Xiaolong Liu, “Observation of Persistent Zero Modes and Superconducting Vortex Doublets in  $\text{UTe}_2$ ,” *arXiv e-prints*, [arXiv:2503.17450](#) (2025), [arXiv:2503.17450 \[cond-mat.supr-con\]](#).
- [43] Anuva Aishwarya, Julian May-Mann, Arjun Raghavan, Laimei Nie, Marisa Romanelli, Sheng Ran, Shanta R. Saha, Johnpierre Paglione, Nicholas P. Butch, Eduardo Fradkin, and Vidya Madhavan, “Magnetic-field-sensitive charge density waves in the superconductor  $\text{UTe}_2$ ,” *Nature* **618**, 928–933 (2023).
- [44] Qiangqiang Gu, Joseph P. Carroll, Shuqiu Wang, Sheng Ran, Christopher Broyles, Hasan Siddiquee, Nicholas P. Butch, Shanta R. Saha, Johnpierre Paglione, J. C. Séamus Davis, and Xiaolong Liu, “Detection of a pair density wave state in  $\text{UTe}_2$ ,” *Nature* **618**, 921–927 (2023).
- [45] C. S. Kengle, J. Vonka, S. Francoual, J. Chang, P. Abbamonte, M. Janoschek, P. F. S. Rosa, and W. Simeth, “Absence of bulk charge density wave order in the normal state of  $\text{UTe}_2$ ,” *Nature Communications* **15**, 9713 (2024).
- [46] Pablo García Talavera, Miguel Águeda Velasco, Makoto Shimizu, Beilun Wu, Georg Knebel, Midori Amano Patino, Gerard Lapertot, Jacques Flouquet, Jean Pascal Brison, Dai Aoki, Youichi Yanase, Edwin Herrera, Isabel Guillamón, and Hermann Suderow, “Surface charge density wave in  $\text{UTe}_2$ ,” *arXiv e-prints*, [arXiv:2504.12505](#) (2025), [arXiv:2504.12505 \[cond-mat.str-el\]](#).